Met. Mater. Int., Vol. 21, No. 1 (2015), pp. 43~53
doi: 10.1007/s12540-015-1006-8

Microstructural Analysis of Cracking Phenomenon Occurring During Cold Rolling of (0.1~0.7)C-3Mn-5Al Lightweight Steels

Seok Su Sohn[1], Byeong-Joo Lee[1], Sunghak Lee[1,*], and Jai-Hyun Kwak[2]

[1]Pohang University of Science and Technology, Center for Advanced Aerospace Materials
Pohang 790-784, Korea
[2]POSCO, Sheet Products & Process Research Group
Technical Research Laboratories, Kwangyang 545-090, Korea

(received date: 26 February 2014 / accepted date: 7 June 2014)

An investigation was conducted into the cracking phenomenon occurring during the cold rolling of lightweight steel plates. Four steels of varying C contents were fabricated and steel plates containing C contents of 0.5 wt% or higher were cracked during the initial stage of the cold rolling. The steels were basically composed of ferrite grains and -carbides in a band shape, but the volume fraction and thickness of κ-carbide band increased as the C content increased. Microstructural observation of the deformed region of fractured tensile specimens revealed that deformation bands were homogeneously formed in wide areas of ferrite matrix in the steels containing C contents of 0.3 wt% or lower, while κ-carbide bands were hardly deformed or cracked. In the steels containing high C contents of 0.5 wt% or higher, on the other hand, microcracks were initiated mostly at fine proeutectoid ferrite located within κ-carbide bands, and were grown further to coalesce with other microcracks to form long cracks. To prevent the cracking, thus, the proeutectoid ferrite should be minimized by the hot rolling in the (α+γ) two phase region. As practical methods, the content of C below 0.5% or Al above 5% was suggested to expand the (α+γ) phase region.

Keywords: ferritic lightweight steel, rolling, fracture, scanning electron microscopy, phase diagram

1. INTRODUCTION

In order to effectively increase fuel efficiency and to decrease CO_2 emission, the reduction in vehicle's weight has been focused in research areas of automotive steels [1-3]. Since automotive steels generally require excellent strength and ductility, highly deformable steels such as transformation induced plasticity (TRIP) steels and twinning induced plasticity (TWIP) steels have been actively developed [4-7]. Recently, ferritic lightweight steels, in which the Al content is higher than 3% and the Mn content is lower than 10%, have also been developed to achieve excellent strength and ductility as well as lightweight effect [8]. The addition of 4~6 wt% of Al generally leads to 6~9% of weight saving in comparison to conventional automotive steels, and offers excellent properties such as strengths above 780 MPa and elongation above 30% [9]. Mn, an austenite stabilizer, raises the amount of austenite at high temperatures [9-11]. Al, a ferrite stabilizer, helps to form a dual phase structure of ferrite and austenite at high temperatures, and promotes the precipitation during cooling [12,13]. When the steels contain hardenability elements such as C, precipitates such as κ-carbides (composition; $(Fe,Mn)_3$-Al-C, perovskite structure) are mainly formed, and the amount of κ-carbides varies with contents of Mn and Al as well as C [14-16].

During the fabrication processes including the hot and cold rolling of these ferritic lightweight steels, κ-carbides are inevitably formed, and then frequently induce the cracking by forming band structures [17,18]. It was thought that the formation of κ-carbides should be inhibited by adding precipitation-hardening elements such as B, Ti, and Nb because κ-carbides had a harmful effect on ductility due to its hardness [10,19], while κ-carbides have been currently used for increasing strengths by controlling their size, fraction, and distribution [20,21]. Though the cracking occurring during the hot or cold rolling is mainly caused by the formation of κ-carbides, very few studies on how alloying elements such as C affect the size, fraction, and distribution of κ-carbides in rolled steel plates have been conducted. Furthermore, the lightweight steels containing about 10 wt% of Mn and Al are newly developed, but their detailed microstructures or deformation and fracture mechanisms are hardly known. Therefore, for the successful development of lightweight steels, the formation of κ-carbides, which can vary with rolling conditions or alloying elements, is essentially verified. From these under-

*Corresponding author: shlee@postech.ac.kr

standings, it is possible to fabricate lightweight steels without any cracks and to improve their mechanical properties simultaneously.

In the present study, four cold-rolled lightweight steel plates having different C contents were fabricated, and the cracking phenomenon occurring during the cold rolling was clarified in relation with microstructural parameters including κ-carbides. The primary causes for the cracking were analyzed by the detailed microstructural examination, and methods to prevent or minimize the cracking were suggested. In addition to the experimental approach, fractions of phases existing at high temperatures were verified by thermodynamic calculations, and the quantitative data were compared with experimentally obtained data.

2. EXPERIMENTAL PROCEDURE

2.1. Lightweight Steels

Four lightweight steels were fabricated by a vacuum induction melting method, and their chemical compositions are Fe-(0.1,0.3,0.5,0.7)C-(3±1)Mn-(5±1)Al-(<0.02)(P+S) (wt%). The steels containing C contents of 0.1, 0.3, 0.5, and 0.7 wt% are referred to as 'C1', 'C3', 'C5', and 'C7', respectively, for convenience. Effects of Al addition on weight reduction are closely related with lattice expansion and low atomic weight of substitutional solutions [9]. The density of the C1~C7 steels was measured to be 6.89~7.07 g/cm^3 by a densitometry (model; Mettler-Toledo XP205, Mettler-Toledo AG, Switzerland) on the basis of the Archimedes Principle, which showed about 10~11% weight reduction in comparison with pure Fe.

After thick plates of 60 mm in thickness were homogenized at 1200 °C for 1 hour, they were hot-rolled at 1100 °C, and the rolling was finished at 900 °C. They were then cooled in a furnace from 650 °C after holding at this temperature for 1 hour in order to simulate a coiling procedure. The hot-rolled steel plates of 3 mm in thickness were rolled at room temperature to make 1-mm-thick steel plates. The cracking phenomenon did not occur during the hot rolling or cooling, but occurred during the cold rolling. It means that the modulus or coefficient (of thermal expansion) mismatch and cooling itself (prior to deformation) are not related with the cracking. Most of the C5 and C7 steel plates were cracked during the initial stage of the cold rolling, whereas the C1 and C3 steel plates were not cracked. Fig. 1 shows examples of cracks occurring during the cold rolling of the C5 and C7 steel plates.

2.2. Microstructural Analysis

The hot-rolled steel plates were polished and etched in a 2% nital solution, and microstructures of longitudinal-transverse (L-T) planes were observed by an optical microscope and a scanning electron microscope (SEM, model; JSM-6330F, JEOL, Japan). Phases present in the steels were identified by X-ray diffraction (XRD), and their volume fractions were measured by an image analyzer (model; SigmaScan Pro ver. 4.0, Jandel Scientific Co.).

2.3. Tension Test

Tensile specimens were obtained from the 1/2 thickness location of the 3-mm-thick hot-rolled plate. Plate-type tensile specimens having a gage length of 50 mm, gage width of 12.5 mm, and gage thickness of 3 mm were prepared in the longitudinal direction, considering that the hot-rolled steel plate was elongated along the longitudinal direction during the cold rolling. They were tested at room temperature at a strain rate of 10^{-3}/s by a universal testing machine (model; Z250, ZWICK GMBH&CO., Germany) of 100 kN capacity. In order to investigate the crack initiation and propagation processes, sub-sized tensile specimens were obtained from the 1/2 thickness location of the 3-mm-thick hot-rolled sheet. Plate-type tensile specimens having a gage length of 12.6 mm, a gage width of 5 mm, and a gage thickness of 1 mm were prepared in the longitudinal direction. The specimens were polished and etched before the tensile test, and the fracture surface and the cross-sectional area beneath fracture surface were observed by an SEM. These SEM micrographs are classified by initial, intermediate, and final stages according to the extent of the distance from the fracture surface.

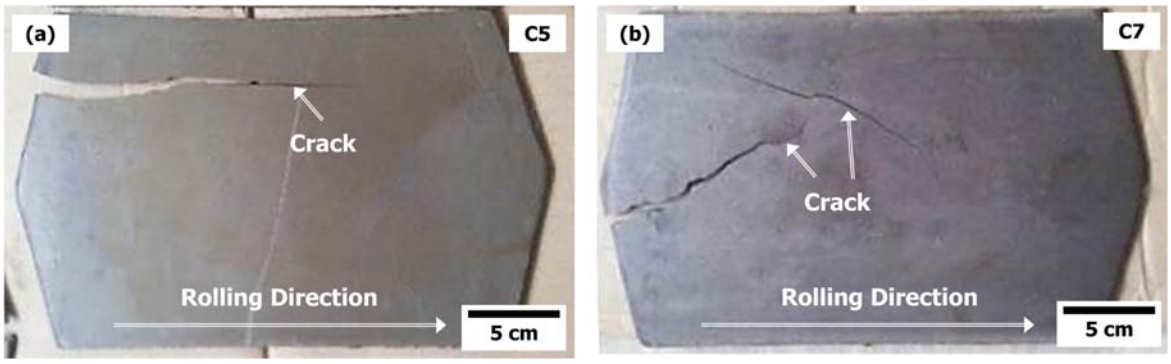

Fig. 1. Optical photographs showing the cracking phenomenon occurring during the cold rolling of the (a) C5 and (b) C7 steel plates.

3. RESULTS

3.1. High-temperature equilibrium phase diagrams

The fractions of phases existing at high temperatures were verified by thermodynamic calculations in order to identify high-temperature phases of the lightweight steels. The Thermo-Calc [22], which is a commercial thermodynamic calculating program, was used for the calculation, and the upgraded version of TCFE2000 [8,23] was used for the thermodynamic database. The fractions of equilibrium phases in the C1 through C7 steels are shown in Figs. 2(a) through (d). The C1 steel mostly consists of ferrite at 1200 °C, and only a small amount of austenites is found (Fig. 2(a)). The amount of ferrite and austenite remains constant as the temperature decreases, but the amount of austenite decreases abruptly from about 700 °C, while κ-carbides begin to precipitate until their content reaches 2% at the coiling temperature of 650 °C. According to the present thermodynamic database [8,23], other phases, *e.g.*, cementite, M_5C_2, and M_7C_3, originating from the Fe-Mn-C ternary system and graphite might appear as stable phases during the equilibrium calculations for these steels, but these phases are not considered in the calculations.

The C3 steel consists of similar amounts of ferrite and austenite at 1200 °C (Fig. 2(b)). The amount of austenite decreases, while that of ferrite increases, as the temperature decreases. At 720 °C, the amount of austenite abruptly decreases, and κ-carbides begin to precipitate. The fraction of precipitated κ-carbide is about 7% at the coiling temperature of 650 °C, which is higher than that in the C1 steel. In the C5 steel, the only austenite is found at 1200 °C, while a small amount of ferrite begins to form at 1100 °C (Fig. 2(c)). When the temperature decreases to 650 °C, the amount of ferrite increases, while that of austenite decreases. κ-carbides start to precipitate at 720 °C, and reaches about 10% at 650 °C. In the C7 steel, the formation behavior of equilibrium phases of austenite, ferrite, and κ-carbide is similar to that in the C5 steel, although the fraction of precipitated κ-carbide is higher (about 15%) than that of the C5 steel (Fig. 2(d)). From these equilibrium phase diagrams, the phase transformation temperatures can be estimated.

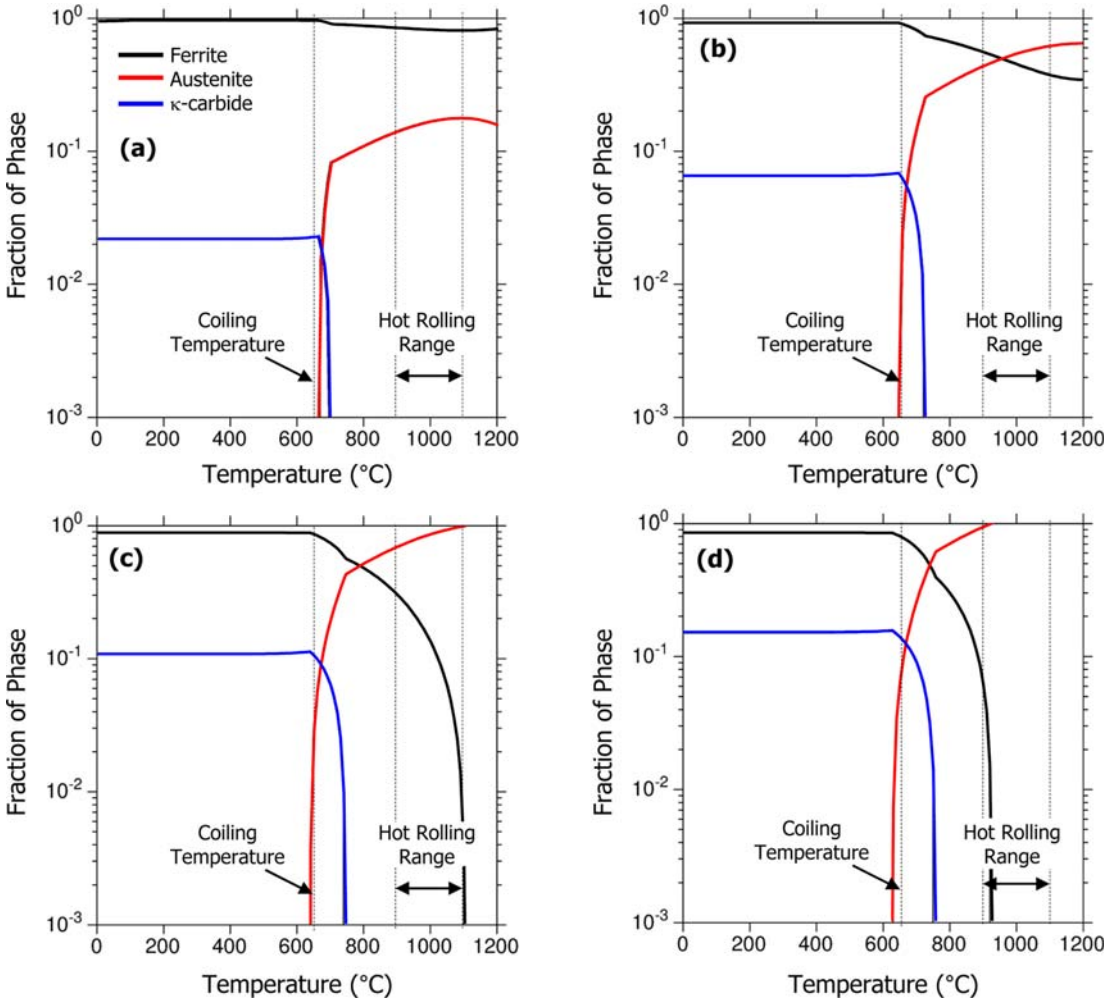

Fig. 2. High-temperature equilibrium phase distribution calculated by using ThermoCalc [8,22,23] for the (a) C1, (b) C3, (c) C5, and (d) C7 steels.

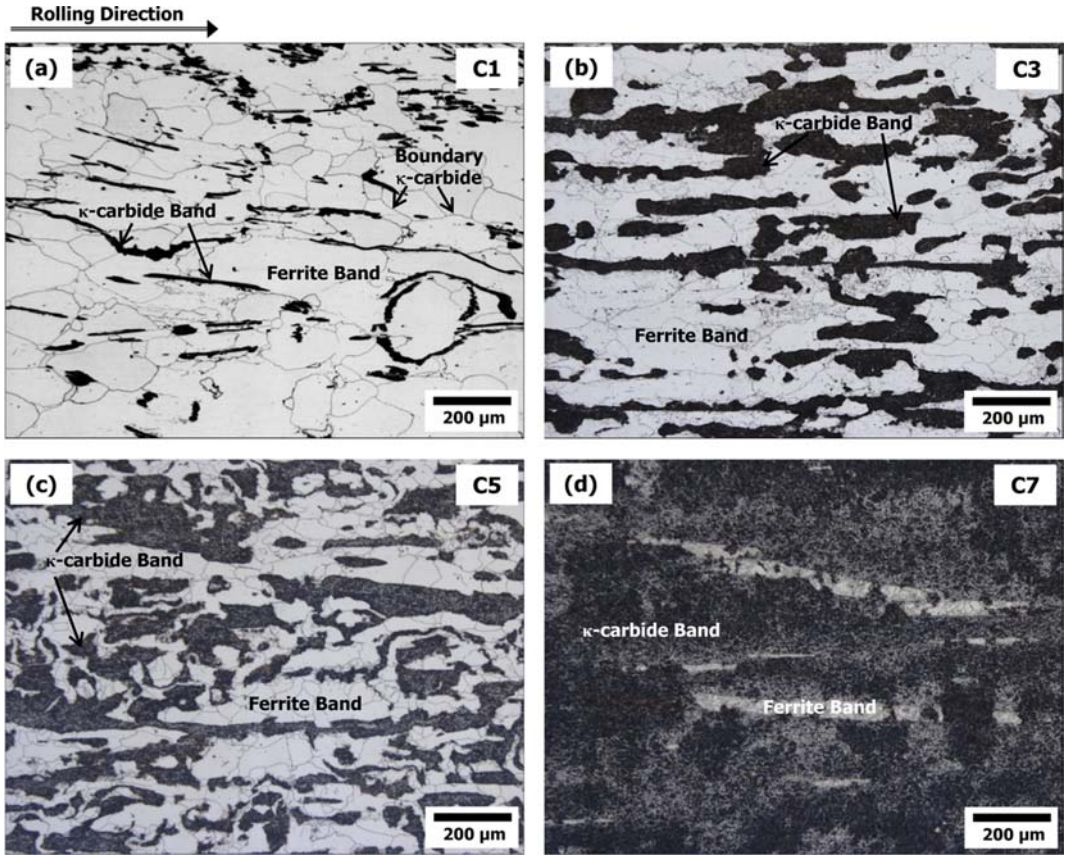

Fig. 3. Optical micrographs (L-T plane) of the (a) C1, (b) C3, (c) C5, and (d) C7 steels. Nital etched.

3.2. Microstructure

Optical micrographs of the hot-rolled C1, C3, C5, and C7 steels are shown in Figs. 3(a) through (d). All the microstructures are parallel to the rolling direction in a banded shape. Black-colored bands in the C1 steel are thinly distributed in the ferrite matrix, and equiaxed ferrite grains of 10~60 μm in size are found between these bands. The thickness of the bands increases in the order of the C1, C3, C5, and C7 steels. Equiaxed ferrite grains of 5~10 μm in size are placed between the bands in the C5 and C7 steels. These black-colored bands contain a number of secondary phases, and the volume fraction of secondary phase bands tends to increase with increasing C content. As secondary phase bands are thicker in the C5 and C7 steels, the volume fraction of κ-carbide band reaches about 50% and 90%, respectively. In the C7 steel, ferrite exists in an isolated island form (Fig. 3(d)).

X-ray diffraction patterns of the steels are provided in Fig. 4. Peaks of ferrite and κ-carbide are observed, and heights of peaks of κ-carbide tend to increase with increasing C content. Thus, secondary phases present in the C1 through C7 steels (Figs. 3(a) through (d)) are κ-carbides, and thus black-colored secondary phase bands are referred to as κ-carbide bands.

Detailed SEM micrographs of the κ-carbide bands are shown in Figs. 5(a) through (d). The C1 steel consists of κ-carbide bands in the ferrite matrix (Fig. 5(a)). Thin film-type κ-carbides are observed along ferrite grain boundaries, as indicated by arrows. Inside the κ-carbide band, lamellar κ-carbides are densely distributed in the ferrite matrix. In the C3 steel, the thickness of κ-carbide band is much larger than that of the

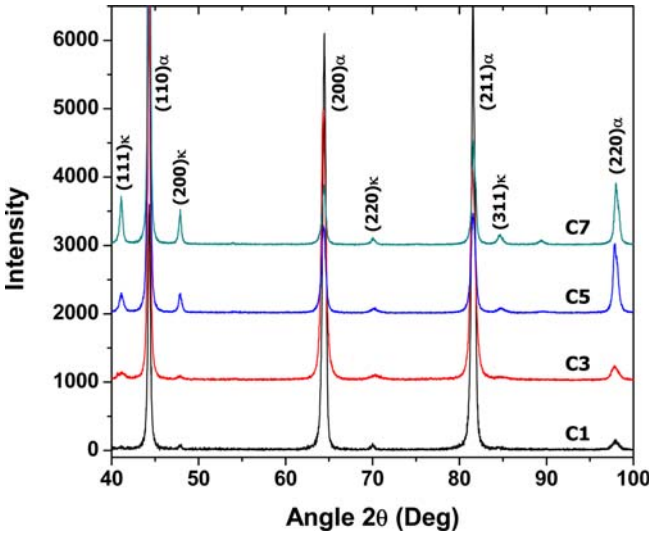

Fig. 4. X-ray diffraction results of the steels.

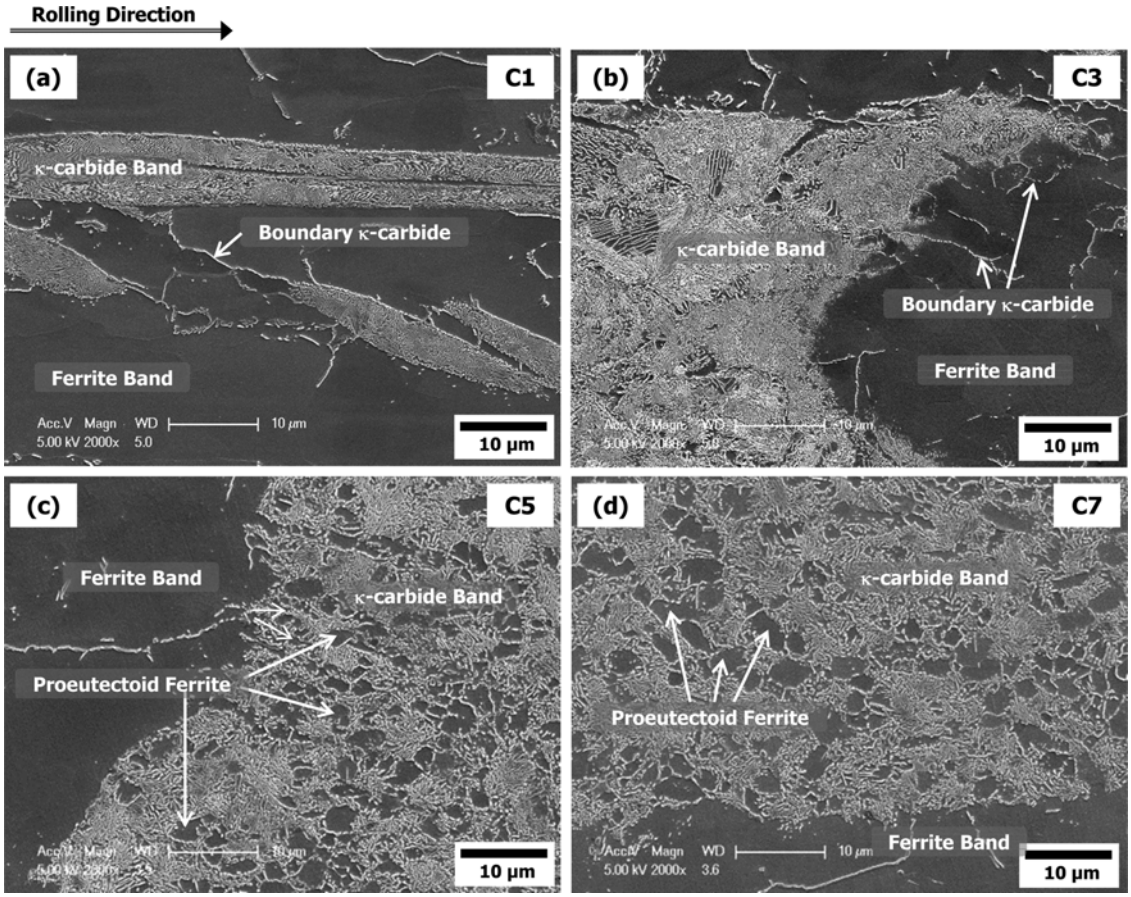

Fig. 5. SEM micrographs (L-T plane) of the (a) C1, (b) C3, (c) C5, and (d) C7 steels. Nital etched.

C1 steel (Fig. 5(b)). κ-carbide bands are well developed in the C5 and C7 steels (Figs. 5(c) and (d)). Inside κ-carbide bands, areas composed of ferrite only without lamellar κ-carbides are observed as indicated by arrows. Their volume fraction is considerably high at about 30% of the total volume of κ-carbide band. Thin film-type grain boundary κ-carbides are also found.

Volume fractions of ferrite matrix and κ-carbide band, together with volume fraction of ferrite existed within κ-carbide band, are summarized in Table 1. The volume fraction of κ-carbide band is 9.5% in the C1 steel, and increases in the order of the C3, C5, and C7 steels with increasing C content, while the fraction of ferrite matrix decreases. The volume fractions of κ-carbide band in the C5 and C7 steels are 51% and 93%, respectively, and override the volume fraction of ferrite matrix. The increasing trend of volume fraction of κ-carbide band in the order of the C1, C3, C5, and C7 steels is approximately coincident with that of fraction of κ-carbide (2, 7, 10, and 15 vol. % in the C1, C3, C5, and C7 steels, respectively) obtained from the equilibrium phase diagrams of Figs. 2(a) through (d) on the basis of the coiling temperature of 650 °C, although there is a large difference between them. This difference can be much reduced when considering that most of κ-carbides are distributed in a shape of a lamellar structure with ferrite inside κ-carbide bands. It is hard to measure the volume fraction of each κ-carbide individually. Also, the calculated fraction is the atomic fraction without considering atomic density, which is different from the measured volume fraction. Thus, the microstructural modifications of the lightweight steels as shown in Figs. 3 and 5 can be explained by the equilibrium phase diagrams and XRD results. Ferrite located within κ-carbide bands is hardly found in the C1 and C3 steels, whereas its volume fraction reaches about 30% of the total volume of κ-carbide band in the C5 and C7 steels (Table 1).

Table 1. Volume fractions of ferrite matrix and κ-carbide band (%)

Steel	Ferrite Matrix	κ-Carbide Band
C1	90.5 ± 4.4	9.5 ± 4.4 (0)*
C3	63.7 ± 6.7	36.3 ± 6.7 (7.7)*
C5	48.6 ± 5.5	51.4 ± 5.5 (28.9)*
C7	7.1 ± 9.1	92.9 ± 9.1 (34.1)*

*( ); volume fraction of ferrite existed within κ-carbide bands.

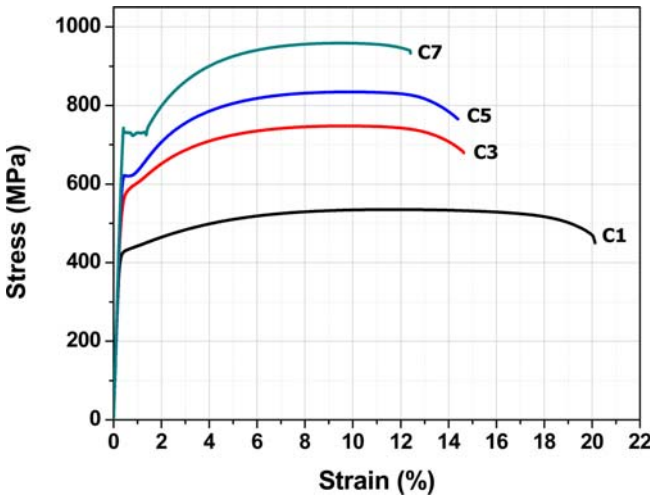

Fig. 6. Room-temperature tensile stress-strain curves of the steels.

Table 2. Room-temperature tensile test results of the lightweight steels

Steel	Yield Strength (MPa)	Tensile Strength (MPa)	Elongation (%)
C1	428.7	535.3	20.1
C3	574.9	747.9	14.6
C5	622.3	834.4	14.4
C7	731.3	958.7	12.4

3.3. Tensile properties

Figure 6 shows room-temperature tensile stress-strain curves, from which tensile properties are summarized in Table 2. The C1 and C3 steels show a continuous yielding behavior, whereas the yield point phenomenon occurs in the C5 and C7 steels. Particularly in the C7 steel, the yield point elongation is clearly shown. This might be related with high carbon content in the C5 and C7 steels, which can induce the formation of Cottrell atmosphere around dislocations. Both the yield and ultimate tensile strengths increase with increasing C content. This is because the volume fraction of κ-carbide band increases in the order of the C1, C3, C5, and C7 steels. The elongation is inversely proportional to the strength trend. The elongation of the C1 steel is 20%, which is much higher than that of the C7 steel.

3.4. Tensile deformation behavior

SEM micrographs of the cross-sectional area beneath the fracture surface of the tensile specimens are shown in Figs. 7 through 10. Here, the rolling direction is parallel to the tensile loading direction. In the initial stage of the C1 steel, a number of deformation bands are initiated inside ferrite grains as marked by arrows (Fig. 7(a)). As the deformation proceeds, deformation bands composed of many parallel slip lines are well developed in wide areas (Fig. 7(b)). It is likely that deformation bands are hardly formed at κ-carbide bands, and that grain boundary κ-carbides hardly work as initiation sites of cracks or voids. With the further deformation, slip lines crossly meet with other slip lines at some areas as marked by arrows. One or two slip lines are deepened inside well-developed deformation bands, and cracks are initiated at the deepened slip lines, thereby leading to the final failure (Fig. 7(c)).

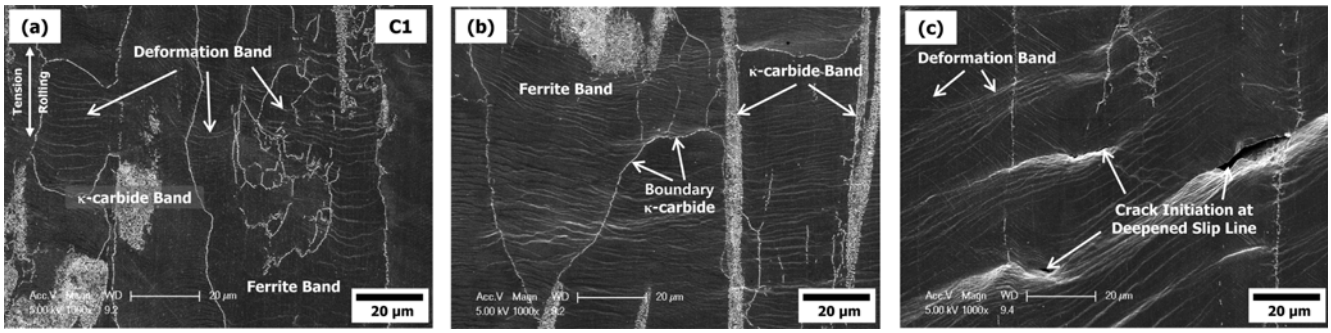

Fig. 7. (a) through (c) SEM micrographs of the cross-sectional area beneath the tensile fracture surface of the C1 steel. Nital etched.

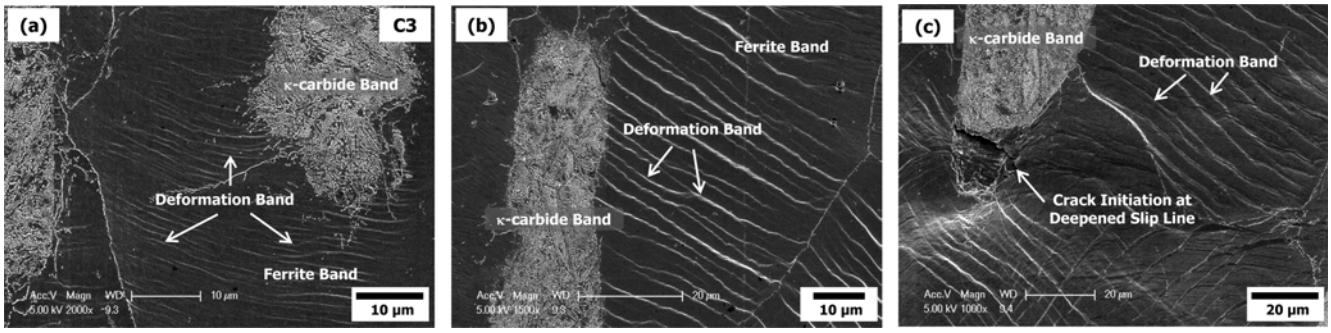

Fig. 8. (a) through (c) SEM micrographs of the cross-sectional area beneath the tensile fracture surface of the C3 steel. Nital etched.

In the C3 steel, the deformation starts at a wide range of ferrite grains, like in the C1 steel (Fig. 8(a)). Deformation bands are formed mainly at ferrite grains, while κ-carbide bands are hardly deformed. Then, several slip lines are deepened inside deformation bands, and propagate into κ-carbide bands, as marked by arrows in Fig. 8(b). These slip lines are deepened further to develop some cracks, which results in the final fracture (Fig. 8(c)).

In the C5 steel whose volume fraction of κ-carbide band is 51%, deformation bands tend to be less actively formed at ferrite grains than in the C1 or C3 steel (Fig. 9(a)). At some areas, grain boundary κ-carbides are voided or cracked as the deformation is concentrated on them as marked by arrows in Fig. 9(b). As the tensile specimen is further strained, microcracks are initiated inside κ-carbide bands (Fig. 9(c)). When the cracked microstructure of κ-carbide bands is magnified, microcracks are frequently found at ferrite regions located within κ-carbide bands, instead of band areas densely populated with lamellar κ-carbides (Fig. 9(d)). This implies that the cracking does not actively take place at lamellar κ-carbides, but does at ferrite regions located within κ-carbide bands.

The deformation behavior of ferrite grains of the C7 steel (volume fraction of κ-carbide band; 93%) is similar to that of the C5 steel. Deformation bands formed at ferrite grains are not well developed as slip lines are hardly deepened (Fig. 10(a)). Inside κ-carbide bands, a number of microcracks are observed as marked by arrows in Fig. 10(b). When the cracked microstructure of κ-carbide bands is magnified, these microcracks are mainly formed at ferrite regions located within κ-carbide band, like in the case of the C5 steel (Fig. 10(c)). Since this ferrite occupies about 30% of total volume of κ-carbide band, the microcracks are readily coalesced with other microcracks to form long cracks inside κ-carbide bands (Fig. 10(d)).

Figs. 11(a) through (d) show SEM fractographs of the fractured tensile specimens. Since deformation bands are well developed in wide areas in the C1 steel whose volume fraction of κ-carbide band is about 10%, the ductile-dimpled fracture mode is predominant in both ferrite and κ-carbide bands (Fig. 11(a)). In the C3 steel, the fracture occurs in a mixed mode of ductile-dimpled fracture and cleavage fracture, and a few secondary cracks are observed on the fracture surface (Fig. 11(b)). As the volume fraction of κ-carbide band reaches 51% in the C5 steel, the quasi-cleavage fracture mode prevails, together with a considerable amount of cleavage mode (Fig. 11(c)). In the C7 steel, the quasi-cleavage fracture mode is also predominant (Fig. 11(d)). Secondary cracks are observed, but are short and shallow. The cleavage fracture mode of the C3, C5, and C7 steels appears in ferrite areas. In the smooth

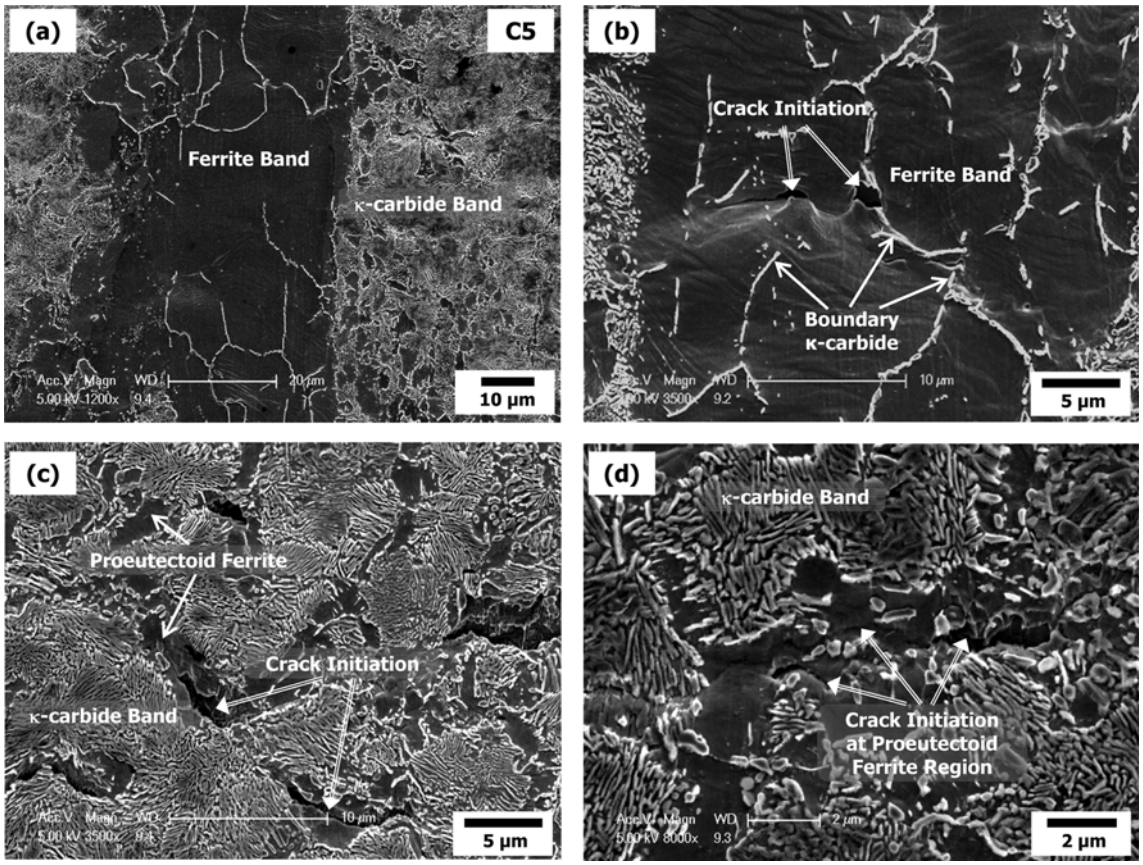

Fig. 9. (a) through (d) SEM micrographs of the cross-sectional area beneath the tensile fracture surface of the C5 steel. Nital etched.

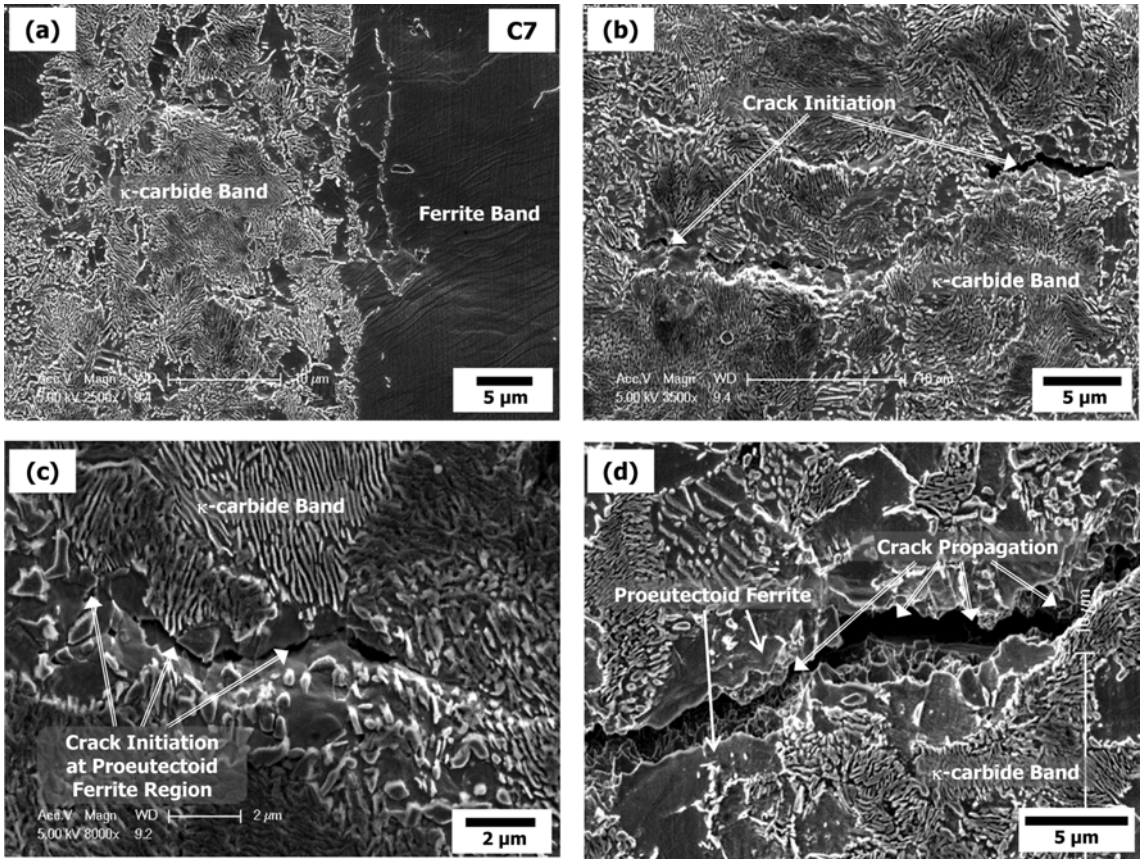

Fig. 10. (a) through (d) SEM micrographs of the cross-sectional area beneath the tensile fracture surface of the C7 steel. Nital etched.

body tensile test, the stress triaxiality may affect the cleavage fracture mode, although it is not seriously large. During the final stage of tensile deformation, interfacial κ-carbides between κ-carbide and ferrite bands or κ-carbides at grain boundaries may act as initiation sites for cleavage fracture, and thus cleavage cracks propagate through ferrite areas.

4. DISCUSSION

During the cold rolling of lightweight steels, the steel plates are often cracked (Fig. 1). Microstructures of the steels are basically composed of ferrite grains and κ-carbides in a band shape, but the morphology, volume fraction, and distribution of κ-carbides affect the cracking behavior in the steels. These differences in κ-carbides are mainly attributed to hot-rolling conditions and alloying elements such as C. In this study, the cracking phenomenon was analyzed, and the analysis results are discussed in detail as follows.

κ-carbides present inside κ-carbide bands are precipitated by the eutectoid reaction, and make a form of a lamellar structure with ferrite [14-17]. However, as observed in the four steels, κ-carbides also exist in a form of particle or thin film at grain boundaries. The precipitation of κ-carbides at grain boundaries takes place before the formation of lamellar κ-carbides when solute atoms such as Mn and C are pre-segregated to grain boundaries [24,25]. Fine proeutectoid ferrite present in the C5 and C7 steels contains a lot of grain boundaries, and thus a considerable number of irregular-shaped coarse κ-carbides are observed in the proeutectoid ferrite regions.

In the C1 steel, thin κ-carbide bands are distributed in the ferrite matrix. According to the observation of the deformed area beneath the fracture surface of the tensile specimen (Figs. 7(a) through (c)), the most critical microstructural parameter affecting the fracture is a deformation band formed mainly at ferrite grains, whereas κ-carbide bands or κ-carbides formed along ferrite grain boundaries do not have much effect on fracture. Since the C1 steel contains a large area of ferrite matrix (volume fraction; 91%), deformation bands are homogeneously formed in wide areas of ferrite matrix when the tensile stress is applied. As the deformation proceeds homogeneously in the wide range of the ferrite matrix, slip lines are deepened inside well-developed deformation bands to reach the fracture (Fig. 7(c)). This relatively homogeneous deformation behavior leads to the final fracture in a ductile dimpled mode. The SEM fractograph in Fig. 11(a) shows that the fracture takes place mainly by a ductile fracture mode. Based on these results, the homogeneous deformation occurs in the wide range of

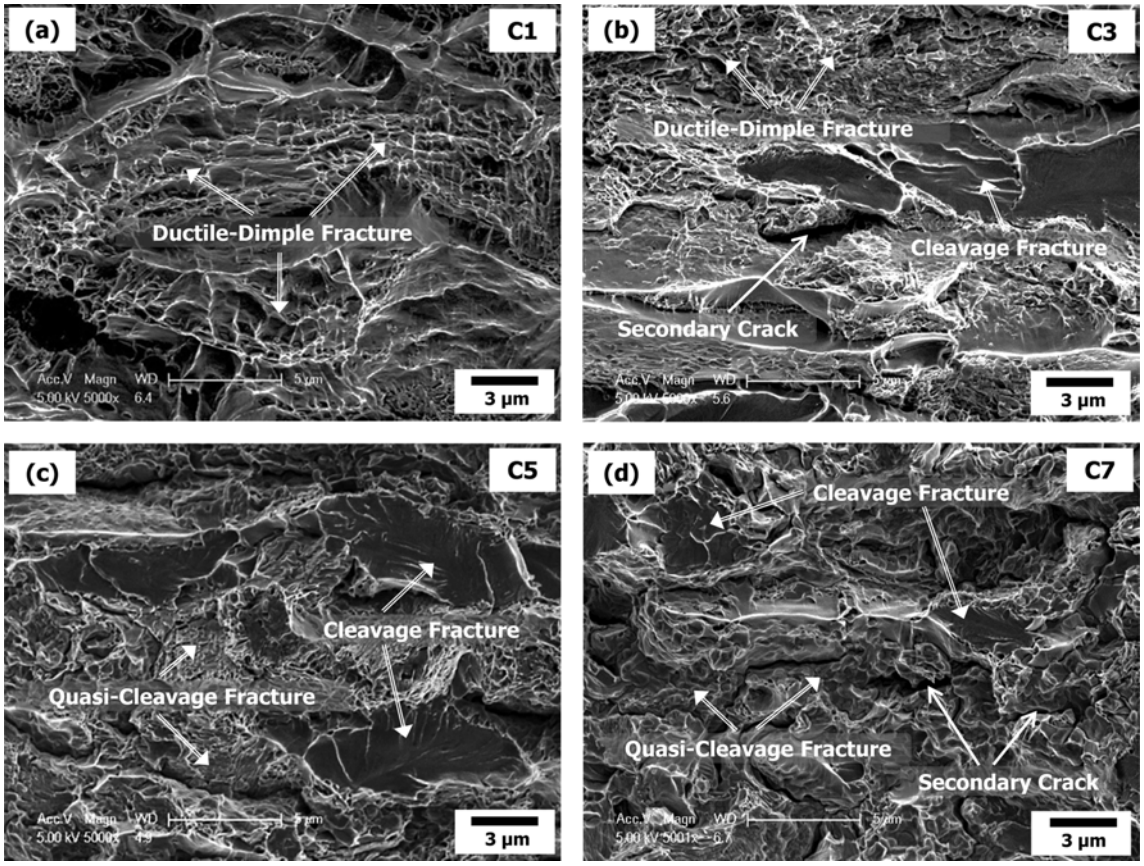

Fig. 11. SEM fractographs of tensile specimens of the (a) C1, (b) C3, (c) C5, and (d) C7 steels.

ferrite matrix under a tensile load, thereby leading to the high tensile ductility of 20%. The yield and tensile strengths are low at about 430 and 535 MPa, respectively, as the tensile specimen is sufficiently deformed even under a relatively low load.

The deformation behavior of the C3 steel is similar to that of the C1 steel because the volume fraction of ferrite matrix is 64%. In the C3 steel, the deformation starts at a wide range of ferrite matrix, like in the C1 steel (Fig. 8(a)). Deformation bands are well developed mainly at the ferrite matrix, while κ-carbide bands are hardly deformed or cracked. The yield and tensile strengths are higher than those of the C1 steel, whereas the elongation is lower.

The formation of κ-carbide bands can be controlled by alloying elements and hot-rolling conditions. Changing the hot-rolling conditions influences the microstructures including ferrite, austenite, and κ-carbide, as shown in high-temperature equilibrium phase diagrams of Figs. 2(a) through (d). However, the control of alloying elements such as C is more desirable and simple, considering the complexity of microstructural changes during the hot rolling. For example, when the C content increases from 0.3% to 0.5 or 0.7%, a considerable amount of κ-carbides are formed, and most of them are observed to be in a lamellar shape inside κ-carbide bands. In the C5 and C7 steels, κ-carbide bands are thickly formed, and their volume fractions are 51 and 93%, respectively. When the tensile load is applied, a considerable load is applied or concentrated to κ-carbide bands as the volume fraction of ferrite matrix is reduced much, and thus κ-carbide bands have a chance to be deformed, unlike in the C3 steel. As κ-carbide bands are deformed, microcracks initiate more at ferrite regions located within -carbide bands than other band areas containing lamellar κ-carbides (Figs. 9(c) and 10(c)). Microcracks are grown further to coalesce with other microcracks to form longer cracks because this ferrite is populated within κ-carbide bands (volume fraction; about 30% of total volume of κ-carbide band). The crack initiation also occurs at grain boundary κ-carbides, but the separation between boundaries is hardly found because boundary κ-carbides are distributed in the relatively broad ferrite matrix area. According to the fractographs in Figs. 11(c) and (d), the fracture occurs mainly by a quasi-cleavage mode, in which rough and fine fracture facets are typically shown, together with a small amount of large cleavage facets. Like in the C5 and C7 steels, thus, the increase in C content promotes the cracking at κ-carbide bands by forming microcracks at ferrite regions within bands. Under tensile loading along the longitudinal direction or the cold rolling, thick carbide bands are more vulnerable to the cracking than the ferrite matrix, and thereby results in the deterioration of

ductility because the tensile specimen or hot-rolled plate is not sufficiently deformed up to a considerably high level of strain.

It is interesting to note that microcracks are rarely initiated at κ-carbide bands composed of lamellar carbides, but that they are mainly initiated at ferrite regions located within κ-carbide bands. This is because the dense carbide bands seem to have a considerable resistance to cracking, like pearlites in conventional plain-carbon ferrite-pearlite steels. Lee *et al*. [26], investigated the primary cause for cracking occurring during cupping of a conventional SG295 steel (composition; 0.134C-0.82Mn-0.29Si-0.017P-0.002S-0.032Al-0.0059N) of ferrite-pearlite microstructure. When external stresses were applied, the strain was markedly localized into carbides distributed along ferrite grain boundaries in an isolated and continuous shape, and microvoids were developed and interconnected to cause the grain boundary fracture. The pearlite structure did not significantly influence the cracking because it was densely populated with lamellar cementites. This result implies that lamellar carbides such as κ-carbides inside bands or cementites inside pearlite grains are hardly cracked if they are densely populated inside a certain area. When ferrite is finely formed in an isolated shape within κ-carbide bands (Figs. 5(c) and (d)), a considerable number of irregular-shaped coarse κ-carbides exist at ferrite regions (Figs. 9(d) and 10(c)). Thus, this ferrite is readily voided or cracked to work as preferential sites for the cracking. In the C5 and C7 steels containing a number of this ferrite, the cracking can frequently occur during the cold rolling.

In order to investigate the formation behavior of these ferrite regions located within κ-carbide bands, which act as preferential initiation sites for the cracking, the detailed interpretation of equilibrium phase diagrams in Figs. 2(a) through (d) is essentially needed. As the hot rolling proceeds at high temperatures, the microstructures containing austenite, ferrite, and κ-carbide are changed. At 1200 °C, the single phase of austenite exists in the C5 and C7 steels, whereas the two phases of austenite and ferrite exist in the C1 and C3 steels. In the C1 and C3 steels, ferrite is continuously formed, while the amount of austenite decreases with decreasing temperature, and a small amount of κ-carbide starts to be precipitated at 700~720 °C as the retained austenite is transformed. Thus, the C1 and C3 steels consist of κ-carbide bands in the ferrite matrix (Figs. 5(a) and (b)). In the C5 and C7 steels, on the other hand, newly formed ferrite is proeutectoid one formed during the hot rolling, because these steels have an austenite single phase at 1200 °C. These proeutectoid ferrite is much smaller than ferrite grains (size; 10~60 μm) formed in the C1 and C3 steels because austenite is deformed in the temperature range of 900~1100 °C during the hot-rolling process. As the temperature decreases further, a considerable amount of κ-carbide starts to be precipitated at 720~750 °C. Since most of the retained austenites are located around fine proeutectoid ferrite, considerably thick κ-carbide bands containing fine proeutectoid ferrite are formed, as shown in Figs. 5(c) and (d).

As aforementioned above, the proeutectoid ferrite region containing a considerable number of irregular-shaped coarse κ-carbide particles is a major cause of the edge-cracking phenomenon. Void and microcracks are initiated at the proeutectoid ferrite region rather than hard lamellar κ-carbide region. In order to suppress the formation of the proeutectoid ferrite, thus, the careful control of manufacturing processes or steel compositions is important. Since the fine proeuctectoid ferrite is formed by the austenite existing single-phase region, it is suggested that the reheating and hot-rolling should be conducted at relatively low temperatures within the (α+γ) two-phase region. It is well known that the hot-rolling in the g single-phase region containing many slip systems provides the better formability than that in the (α+γ) two-phase region. In the Fe-Mn-Al-C lightweight steels having κ-carbides, the hot-rolling cracking is not a serious problem even during the hot-rolling process in the (α+γ) two-phase region. Thus, the hot-rolling in the (α+γ) two-phase region would be better than that in the g single-phase region, if considering the cold-rolling cracking originated from proeutectoid ferrite regions. However, this method (the hot-rolling at relatively low temperatures within the (α+γ) two-phase region) is not a practical solution in real time processing. As a practical solution, the addition of ferrite stabilization elements such as Al above 5% is recommended to expand the ferrite region at high temperatures. However, the appropriate combination of alloying elements is needed because the further addition of Al changes the volume fraction and transformation temperature of κ-carbides. Therefore, systematic studies on phase-transformation mechanisms involved in local microstructural change during the hot rolling and cooling as well as microstructural analysis of the primary causes for the cracking are still required. Since only the steels containing different C contents are compared in this study, microstructures of lightweight steels fabricated under various chemical compositions and hot-rolling conditions are to be analyzed, and more fundamental correlation study between microstructures and deformation and fracture mechanisms is to be investigated in the future.

5. CONCLUSIONS

In the present study, the cracking phenomenon occurring during the cold rolling of four lightweight steels was investigated in relation with microstructure.

(1) Phases formed at high temperatures were analyzed from thermodynamically calculated equilibrium phase diagrams. Fractions of phases and phase transformation temperatures obtained from the phase diagrams were well matched with the results obtained from actual microstructures.

(2) The microstructures of the steels were basically composed of ferrite grains and κ-carbides in a banded shape, but

the morphology, volume fraction, and distribution of them were different. The C1 steel consisted mostly of thin κ-carbide bands in the ferrite matrix, and thin film-type κ-carbides were located along ferrite grain boundaries. As the C content increased, the volume fraction and thickness of κ-carbide band increased, while fine proeutectoid ferrite existed in an isolated island form in the C5 and C7 steels.

(3) Microstructural observation of the deformed region of fractured tensile specimens revealed that deformation bands were homogeneously formed in wide areas of ferrite matrix in the C1 and C3 steels, while κ-carbide bands were hardly deformed or cracked. In the C5 and C7 steels, on the other hand, microcracks were initiated more at fine proeutectoid ferrite located within κ-carbide bands than other band areas containing lamellar κ-carbides, and were grown further to coalesce with other microcracks to form long cracks.

(4) In order to prevent the cracking occurred during the cold rolling, it was recommended that the reheating and hot rolling should be conducted in the (α+γ) two phase region for minimizing the formation of fine proeutectoid ferrite. However, the hot rolling in the two phase region might cause unpredictable problems of the productivity reduction or the microstructural complexity. As practical methods for preventing the cracking, the content of C below 0.5% or the content of Al above 5% was suggested to expand the (α+γ) phase region.

ACKNOWLEDGMENTS

This work was supported by the Ministry of Knowledge Economy under a grant No. 10031723-2011-21. The authors would like to thank Professor Nack J. Kim and Mr. Hyuk-Joong Lee of POSTECH for their help with the alloying effect and microstructural analysis.

REFERENCES

1. P. J. Jacques, *Curr. Opin. Solid State Mater. Sci.* **8**, 259 (2004).
2. S. Zaefferer, J. Ohlert, and W. Bleck, *Acta Mater.* **52**, 2765 (2004).
3. I. B. Timokhina, P. D Hodgson, and E. V. Pereloma, *Metall. Mater. Trans. A* **35A**, 2331 (2004).
4. J. Bouquerel, K. Verbeken, and B. C. De Cooman, *Acta Mater.* **54**, 1443 (2006).
5. S. Vercammen, B. Blanpain, B. C. De Cooman, and P. Wollants, *Acta Mater.* **52**, 2005 (2004).
6. J. E. Jung, J. Park, J.-S. Kim, J. B. Jeon, S. K. Kim, and Y. W. Chang, *Met. Mater. Int*. **20**, 27 (2014).
7. J.-S. Kim, J. B. Jeon, J. E. Jung, K.-K. Um, and Y. W. Chang, *Met. Mater. Int*. **20**, 27 (2014).
8. K.-G. Chin, H.-J. Lee, J.-H. Kwak, J.-Y. Kang, and B.-J. Lee, *J. Alloys Compd.* **505**, 217 (2010).
9. G. Frommeyer and U. Brüx, *Steel Res. Int.* **77**, 627 (2006).
10. G. Frommeyer and J.A. Jiménez, *Metall. Mater. Trans. A* **36A**, 295 (2005).
11. B. Hwang, T.-H. Lee, J.-H. Shin, and J.-W. Lee, *Korean J. Met. Mater.* **52**, 21 (2014).
12. H. Kim, D.-W. Suh, and N. J. Kim, *Sci. Technol. Adv. Mater.* **14**, 1 (2013).
13. D.-W. Suh, S. J. Park, T. H. Lee, C. S. Oh, and S. J. Kim, *Metall. Mater. Trans. A* **41A**, 397 (2010).
14. H. Huang, D. Gan, and P. W. Kao, *Scr. Metall. Mater.* **30**, 499 (1994).
15. W. K. Choo, J. H. Kim, and J. C. Yoon, *Acta Mater.* **45**, 4877 (1997).
16. C. L. Lin, C. G. Chao, H. Y. Bor, and T. F. Liu, *Mater. Trans.* **51**, 1084 (2010).
17. S. Y. Han, S. Y. Shin, S. Lee, N. J. Kim, J.-H. Kwak, and K.-G. Chin, *Metall. Mater. Trans. A* **42A**, 138 (2011).
18. F. D'Errico, *J. Fail. Anal. Preven.* **10**, 351 (2010).
19. K. T. Luo, P. W. Kao, and D. Gan, *Mater. Sci. Eng.* **A151**, L15 (1992).
20. Y. Kimura, K. Handa, K. Hayashi, and Y. Mishima, *Intermetallics* **12**, 607 (2004).
21. Y. Kimura, K. Hayashi, K. Handa, and Y. Mishima, *Mater. Sci. Eng.* **A329-331**, 680 (2002).
22. B. Sundman, B. Jansson, and J.-O. Andersson, *Calphad* **9**, 153 (1985).
23. B.-J. Lee and B. Sundman, *Thermo-calc database TCFE2000*, 1999, KTH, Stockholm.
24. J. Jeong, C.-Y. Lee, I.-J. Park, and Y.-K. Lee, *J. Alloys Compd.* **574**, 299 (2013).
25. P. Kratochvíla, F. Dobešb, and V. Vodičkovác, *Intermetallics*, **17**, 39 (2009).
26. S. Lee, C. G. Lee, D. Kwon, S.-H. Park, and N. J. Kim, *Metall. Mater. Trans. A* **27A**, 1241 (1996).